Received: 22 February 2019 | Accepted: 26 August 2019

DOI: 10.1002/jcp.29182

ORIGINAL RESEARCH ARTICLE

Journal of Cellular Physiology WILEY

Deacetylation of LAMP1 drives lipophagy-dependent generation of free fatty acids by *Abrus* agglutinin to promote senescence in prostate cancer

Prashanta Kumar Panda[1] | Srimanta Patra[1] | Prajna Paramita Naik[1] | Prakash Priyadarshi Praharaj[1] | Subhadip Mukhopadhyay[1] | Biswa Ranjan Meher[2] | Piyush Kumar Gupta[3] | Rama S. Verma[3] | Tapas K. Maiti[4] | Sujit K. Bhutia[1]

[1]Department of Life Science, National Institute of Technology Rourkela, Rourkela, India

[2]PG Department of Botany, Berhampur University, Brahmapur, India

[3]Department of Biotechnology, Bhupat and Jyoti Mehta School of Biosciences, Indian Institute of Technology Madras, Chennai, India

[4]Department of Biotechnology, Indian Institute of Technology Kharagpur, Kharagpur, India

Correspondence
Sujit Kumar Bhutia, Department of Life Science, National Institute of Technology Rourkela, Rourkela-769008, Odisha, India.
Email: sujitb@nitrkl.ac.in and bhutiask@gmail.com

Funding information
Science and Engineering Research Board (SERB), Grant/Award Number: EMR/2016/001246; Council for Scientific and Industrial Research, Grant/Award Number: 37(1715)/18/EMR-II

Abstract

Therapy-induced senescence in cancer cells is an irreversible antiproliferative state, which inhibits tumor growth and is therefore a potent anti-neoplastic mechanism. In this study, low doses of *Abrus* agglutinin (AGG)-induced senescence through autophagy in prostate carcinoma cells (PC3) and inhibited proliferation. The inhibition of autophagy with 3-methyl adenine reversed AGG-induced senescence, thus confirming that AGG-triggered senescence required autophagy. AGG treatment also led to lipophagy-mediated accumulation of free fatty acids (FFAs), with a concomitant decrease in the number of lipid droplets. Lalistat, a lysosomal acid lipase inhibitor, abrogated AGG-induced lipophagy and senescence in PC3 cells, indicating that lipophagy is essential for AGG-induced senescence. The accumulation of FFAs increased reactive oxygen species generation, a known facilitator of senescence, which was also reduced in the presence of lalistat. Furthermore, AGG upregulated silent mating type information regulator 2 homolog 1 (SIRT1), while the presence of sirtinol reduced autophagy flux and the senescent phenotype in the AGG-treated cells. Mechanistically, AGG-induced cytoplasmic SIRT1 deacetylated a Lys residue on the cytoplasmic domain of lysosome-associated membrane protein 1 (LAMP1), an autolysosomal protein, resulting in lipophagy and senescence. Taken together, our findings demonstrate a novel SIRT1/LAMP1/lipophagy axis mediating AGG-induced senescence in prostate cancer cells.

KEYWORDS
Abrus agglutinin, free fatty acid, LAMP1, lipophagy, reactive oxygen species, senescence, SIRT1

1 | INTRODUCTION

Cellular senescence is an irreversible state wherein cells cease to divide; diploid somatic cells have a limited lifespan due to telomere shortening, a phenomenon known as replicative senescence (Hayflick, 1965). In addition, senescence is the primary response to DNA damage during transient cellular transformation is called oncogene-induced senescence (Barnoud, Schmidt, Donninger, &

Abbreviations: AGG, *Abrus* agglutinin; CDKI, cyclin-dependent kinase inhibitor; DMSO, dimethylsulfoxide; FFA, free fatty acids; LAMP1, lysosome-associated membrane protein 1; MD, molecular dynamics; PAGE, polyacrylamide gel electrophoresis; PBS, phosphate-buffered saline; PCNA, proliferating cell nuclear antigen; ROS, reactive oxygen species; RIP II, ribosome inhibiting protein; SDS, sodium dodecyl sulfate; SIRT1, silent mating type information regulator 2 homolog 1; TIS, therapy-induced senescence; 3-MA, 3-methyl adenine.

Clark, 2017), as well as of cancer cells to chemotherapy and radiation. The latter is called premature or therapy-induced senescence (TIS), which apart from inhibiting cancer cell proliferation, also activates the antitumor immune response in patients that acts as a backup response when apoptosis is disabled (Gewirtz, Holt, & Elmore, 2008; Schmitt et al., 2002; Vargas, Feltes, Poloni Jde, Lenz, & Bonatto, 2012; Xue et al., 2007). TIS is an important antitumor mechanism against cancers of limited lethality (Gewirtz, 2013). Earlier studies have shown an upregulation of autophagy-related genes during oncogene-induced senescence, while inhibition of autophagy delays the appearance of senescent cells (Young et al., 2009). Autophagy is a catabolic process wherein damaged cells and organelles are engulfed by specialized vesicles called autophagosomes To recycle the components for de novo biosynthesis and provide energy (Mukhopadhyay, Panda, Sinha, Das, & Bhutia, 2014; Panda et al., 2015). Both autophagy and senescence are cellular responses to stimuli like DNA damage, oxidative and oncogenic stress as well as telomere shortening, and autophagy plays a dual role in facilitating senescence. In addition, autophagy and senescence have overlapping, complementary and even opposing functions while modulating anticancer therapeutic response (Gewirtz, 2013).

Abrus agglutinin (AGG) is a 134-kD type II ribosome-inactivating lectin isolated from the seeds of *Abrus precatorius*. It is a homodimer glycoprotein consisting of two 30 kDa A chains and two 31 kDa B chains linked through disulfide bonds. The B chain has a high specificity toward β-galactosides that facilitates cellular translocation of AGG, whereas the A chain inhibits protein synthesis (Bagaria, Surendranath, Ramagopal, Ramakumar, & Karande, 2006; Hegde, Maiti, & Podder, 1991). We have previously highlighted the potent anti-neoplastic actions of AGG via apoptosis induction (Mukhopadhyay, Panda, Das, et al., 2014; Naik et al., 2016; Sinha, Panda, Naik, Das, et al., 2017; Sinha, Panda, Naik, Maiti, & Bhutia, 2017), autophagy-dependent cell death (Panda et al., 2017), Inhibition of tumor angiogenesis (Naik et al., 2016) and immunoactivation (Bhutia, Mallick, & Maiti, 2009; Ghosh, Bhutia, Mallick, Banerjee, & Maiti, 2009). In a recent study, we found that AGG-induced autophagy in cervical cancer cells following endoplasmic stress by inhibiting the Akt/PH domain (Panda et al., 2017), and triggered PUMA-induced selective mitochondrial elimination in glioblastoma cells to initiate apoptosis through ceramide generation (Panda, Naik, Meher, et al., 2018). In addition, AGG-induced autophagy-mediated differentiation in colon cancer stem cells (Panda, Naik, Praharaj, et al., 2018), resulting in a significant antitumor effect. However, the potential role of AGG in inducing senescence, as well as the underlying mechanism, is unclear.

Silent mating type information regulator 2 homolog 1 (sirtuin 1 or SIRT1), an NAD^+-dependent nuclear histone deacetylase, epigenetically regulates transcription, metabolism, stress response, DNA repair, senescence, autophagy, and apoptosis during aging and cancer (Chua et al., 2005; Fang & Nicholl, 2011; T. Zhang & Kraus, 2010). In mammals, SIRT1 levels increase following nutrient starvation, which deacetylates non-histone proteins and allows mammalian cells to conserve energy and survive under stress (Shan et al., 2017). Furthermore, it has been reported that under oxidative stress, SIRT1 positively regulates autophagy and mitochondrial function through the class III PI3K/Beclin-1 and mTOR pathway (Ou, Lee, Huang, Messina-Graham, & Broxmeyer, 2014). SIRT1 can also initiate autophagy directly by deacetylating the autophagy-related nuclear LC3 protein at Lys49 and Lys51, as well as Atg5, Atg7, and Atg8 during serum starvation (R. Huang et al., 2015). SIRT1 frequently shuttles between the nucleus and cytoplasm depending on the stimuli (Gewirtz, 2013), and is mainly localized to the cytoplasm of cancer cells where it maintains PI3K-induced proliferation (Byles et al., 2010). Earlier studies also show that SIRT1 knockdown diminished the senescent phenotype in response to genotoxic stress (Chua et al., 2005). Taken together, SIRT1 is likely involved in the cross-talk between senescence and autophagy in cancer cells.

The aim of this study, therefore, was to investigate the effects of AGG on a human prostate carcinoma cell line (PC3), and the possible mechanistic role of SIRT1. We found that AGG accelerated TIS in prostate cancer cells via an autophagy-dependent pathway. Mechanistically, AGG-induced SIRT1 activation led to the deacetylation of the lysosome-associated membrane protein 1 (LAMP-1), a lysosomal membrane glycoprotein which plays an important role in lysosomal integrity for cellular degradation and metabolism. In addition, AGG also induced lipophagy that led to the accumulation of free fatty acids (FFAs), and increased reactive oxygen species (ROS) production, while the inhibition of lipophagy suppressed AGG-induced senescence in a ROS-dependent manner. Taken together, AGG-induced lipophagy leading to TIS is a potent tumor suppressor mechanism.

2 | MATERIALS AND METHODS

2.1 | Reagents

X-gal or 5-bromo-4-chloro-3-indolyl β-D-galactopyranoside (B4252), 4′,6-diamidino-2-phenylindole dihydrochloride (DAPI; D9542), 3-methyl adenine (3-MA; M9281), Oil Red O (O0625), Sirtinol (S7942), and lysosome-associated membrane protein 1 (LAMP1; SAB3500285) and free fatty acid quantitation kit (MAK044) were purchased from Sigma–Aldrich (St. Louis, MO). Lalistat was procured from Chemical Synthesis and Drug Discovery Facility (University of Notre Dame). HCS LipidTOX™ Green (H34475), NE-PER™ Nuclear and Cytoplasmic Extraction Reagents (78835) were purchased from Thermo Fisher Scientific (Waltham, MA), and the β-galactosidase staining kit (9860S) from Cell Signaling and Technologies (Danvers, MA). The anti-LC3 antibody (NB100-2220) was obtained from Novus Biological (Littleton, CO), and antibodies against p21 (556430), proliferating cell nuclear antigen (PCNA; 610664), pRb (554136), and cyclin B1 (554179) were purchased from BD Biosciences (Franklin Lakes, NJ). SIRT1 (2493S), BECN1 (3738S), Atg5 (2630S), cyclin D1 (2929S), and acetylated lysine (9681S) were procured from Cell Signaling Technologies (CST, Danvers, MA), β-actin (A2066) from Sigma–Aldrich (St. Louis, MO), perilipin2 (MAB76341-SP) from R&D Systems (MN).

2.2 | Cell culture

The human prostate cancer cell line PC3 was obtained from the National Centre for Cell Science (NCCS, Pune, India). The PC3 cells were cultured in Dulbecco's modified Eagle's medium-F12 supplemented with antibiotics/antimitotics and 10% fetal bovine serum at 37°C under 5% CO_2.

2.3 | AGG purification

AGG was isolated from *A. precatorius* seeds by 30–90% ammonium sulfate fractionation, followed by lactamyl Sepharose affinity chromatography. The protein bound to the lactamyl Sepharose column was eluted with 0.4 M lactose. The highly purified AGG was then separated from the toxic abrin by Sephadex G-100 gel-permeation chromatography. The purity of the isolated AGG was confirmed by sodium dodecyl sulfate polyacrylamide gel electrophoresis (SDS-PAGE), native-PAGE, and gel permeation HPLC, and its lectin activity by hemagglutination assay (Hegde et al., 1991).

2.4 | Senescence-associated-β-galactosidase (SA-β-gal) staining

SA-β-gal activity was assessed in cells treated with AGG for 72 hr using a commercially available staining kit according to the manufacturer's instructions. The senescent cells were identified by blue staining under a light microscope, and 100 cells were counted for statistical analysis (Mukhopadhyay, Panda, Behera, et al., 2014).

2.5 | Cell cycle analysis

AGG-treated PC3 cells were harvested and fixed in 70% ethanol at −20°C, washed with ice-cold phosphate-buffered saline (PBS; 10 mM, pH 7.4), and resuspended in 200 μl PBS. The fixed cells were incubated with 20 μl DNase-free RNase (10 mg/ml) and 20 μl propidium iodide (PI; 1 mg/ml) at 37°C for 1 hr in the dark. The distribution of cells in the different cell cycle phases was analyzed using BD ACCURI C6 flow cytometer and FCS EXPRESS software (Sinha, Panda, Naik, Das, et al., 2017).

2.6 | Western blot analysis and immunoprecipitation

Harvested PC3 cells were lysed with a protein lysis buffer, and about 50 μg protein per sample was separated by SDS-PAGE and transferred onto a nitrocellulose membrane. After blocking with 5% BSA (in PBST) at room temperature for 1 hr, the blots were incubated overnight with the respective antibodies (LC3, SIRT1, LAMP1, acetylated lysine, p21, pRb, PCNA, and actin) at 4°C, followed by incubation with secondary antibodies for 1 hr at room temperature. The positive bands were detected using a chemiluminescence method and quantified by the ImageJ software (Naik et al., 2016). For immunoprecipitation, the cell lysates were incubated with the aforementioned antibodies followed by binding with protein A dynabeads (Invitrogen, CA; 10006D) and downstream western blot was performed as described earlier (Panda, Naik, Praharaj et al., 2018).

2.7 | Quantification of total lipid content and FFAs

AGG-treated cells were washed with PBS and fixed in formalin for 10 min at room temperature. After washing twice with double distilled water (ddH_2O) and then with 60% isopropanol, the cells were dried completely and incubated with the Oil Red O dye at room temperature for 10 min. After washing with ddH_2O, the dye was eluted with 1 ml 100% isopropanol and incubated for 10 min with gentle shaking. The optical density of the eluents was measured at 500 nm, and the FFAs were quantified according to the manufacturer's instructions (Mukhopadhyay et al., 2017).

2.8 | Immunofluorescence

PC3 cells were fixed, permeabilized, and incubated overnight with the primary antibodies, and then with the Alexa Fluor-labeled secondary anti-rabbit and/or anti-mouse antibodies. For lipid droplet (LD) staining, the cells were rinsed with PBS, fixed with formaldehyde, and stained with LipidTOX Green for 30 min. The stained cells were observed using a confocal laser microscope (Leica TCS SP8).

2.9 | Measurement of autophagic flux by tandem fluorescent-tagged LC3 (tfLC3) plasmid transfection

PC3 cells were transfected with ptfLC3 (Addgene plasmid 21074) using Lipofectamine 2000 reagent (Gibco) according to the manufacturer's instructions and treated with AGG as described. Autophagosome and autolysosome formation was detected as fluorescent-tagged LC3 punctae by confocal microscopy (Olympus FV−1000, ×630). The autophagic flux was quantified by counting the RFP^+GFP^+ (yellow) autophagosome and RFP^+GFP^- (red) autolysosomes punctae. A minimum of 100 tfLC3-transfected cells were counted per experiment.

2.10 | Isolation of nuclear and cytoplasmic proteins

PC3 cells (7×10^5 cells) were cultured in 60 mm cell culture discs in RPMI-1640 medium supplemented with 10% serum and penicillin/streptomycin. Following suitable treatment, the cells were harvested with trypsin-ethylenediaminetetraacetic acid and then centrifuged at 500*g* for 5 min. The nuclear and cytoplasmic fractions were isolated using the NE-PER Nuclear and Cytoplasmic Extraction Reagents kit (Thermo #78835) according to the manufacturer's instructions. Briefly, ice-cold CER I reagent was added to the cell pellets, which were vortexed and kept on ice for 10 min. Ice-cold CER II was then added, and the samples were centrifuged (~16,000*g*) after 10 min to separate the cytoplasmic fraction. The remaining insoluble (pellet) fraction was resuspended in ice-cold NER, vortexed and kept on ice for 10 min. The samples were again centrifuged at about 16,000*g* for 10 min to isolate the nuclear fraction. Tubulin and Lamin B1 were

used as the respective cytoplasmic and nuclear markers for quality control (Yang et al., 2018).

2.11 | Modeling SIRT1–LAMP1 complex through docking and molecular dynamics simulation

The crystal structures of human SIRT1 protein (opened state) was obtained from the Protein Data Bank (PDB ID: 4IG9; Davenport, Huber, & Hoelz, 2014). Due to the unavailability of a complete and high-resolution crystal structure of the LAMP1 protein (Eskelinen, 2006), its putative 3D structure was predicted and modeled using the Phyre-2 software that was comprised of 190 residues. The docking algorithm was then used to locate the optimal configuration of the LAMP1 protein near the binding site of SIRT1. Initially, the LAMP1 domain was positioned near the binding site, and the docking algorithm was performed by the Cluspro−2 server. The docked complex structure with the highest score was then considered for the molecular dynamics (MD) simulation (Panda et al., 2017).

2.12 | Statistical analysis

All data are representative of at least three independent experiments and presented as the mean ± standard deviation. Different groups were compared using either Student's *t* test or a one-way analysis of variance, Kruskal–Wallis test with Dunn's multiple group comparison as appropriate.

3 | RESULTS

3.1 | AGG induces senescence and growth arrest in PC3 cells

The TIS especially irreversible senescence with therapeutic agents and radiation is an important antitumor mechanism against cancers with limited toxicity (Gewirtz, 2013). To investigate the antitumor activity of AGG at lower doses, PC3 cells were treated with different concentrations of AGG (25, 50, and 100 ng/ml) for 72 hr, and induction of senescence and growth arrest was analyzed. AGG increased the percentage of SA-β-gal-positive cells in a dose-dependent manner (Figure 1a) from 6.5 ± 0.5% in the untreated controls to 12.0 ± 1.5%, 28.7 ± 4.3%, and 40.8 ± 5.5% at the 25, 50, and 100 ng/ml doses, respectively (Figure 1b). In addition, a time-dependent increase was also seen in SA-β-Gal staining after AGG treatment (Figure 1c,d). Apart from positive SA-β-gal staining, the characteristic flat and hypertrophic morphology of senescent cells were also observed in the AGG-treated PC3 cells.

PI staining showed a dose-dependent increase in the proportion of AGG-treated cells in the G0/G1 phase, without any significant changes in other phases of the cell cycle (Figure 1e,f). Furthermore, there was a significant dose-dependent decrease in cyclins D1 and B1 levels, and an increase in p21 levels in the AGG-treated cells compared with the untreated control. P21 is an important cyclin-dependent kinase inhibitor (CDKI), which plays a vital role in growth arrest and senescence (Goehe et al., 2012), and both cyclins are known to decrease during senescence (Y. H. Huang et al., 2014). Finally, AGG-treated cells showed a significant decrease in the proliferating cell nuclear antigen (PCNA) and phosphorylated retinoblastoma (pRb) expression in a dose-dependent manner (Figure 1g,h). Taken together, AGG induces TIS and G0/G1 phase arrest in prostate cancer cells.

3.2 | AGG-induced autophagy regulates senescence in PC3 cells

To determine the relationship between autophagy and senescence in prostate cancer cells following low dose AGG exposure, we first analyzed autophagy induction in terms of endogenous LC3 levels in the AGG-insulted PC3 cells. AGG was shown to increase lipidation of LC3 results in an increased LC3-II/LC3-I ratio, increased the levels of the pro-autophagic proteins including Beclin-1 and ATG5 in a dose-dependent manner (Figure 2a,b). Furthermore, the expression of p62, an autophagosome cargo protein required for autophagic clearance, was downregulated in the AGG-treated cells. The mRFP-GFP tfLC3 was used to monitor autophagic flux, which revealed a significant increase in the red fluorescent punctae with a dose of 100 ng/ml AGG indicating autophagy activation (Figure 2c,d). Interestingly, we have analyzed autophagic flux in presence of chloroquine (CQ), lysosomal inhibitor, and our data showed that AGG-induced LC3 accumulation and decrease in p62 level was increased as compared with AGG-treated group in PC3 cells (Figure 2e,f) confirming induction of autophagy.

To establish the functional link between autophagy and senescence, we inhibited autophagy in the PC3 cells using the class III PI3K inhibitor 3-MA and found a significant reduction in SA-β-Gal staining even in the presence of AGG (Figure 3a,b). Interestingly, the presence of 3-MA decreased the expression of p21 and increased that of PCNA in the AGG-treated cells (Figure 3c,d). In addition, our data showed that AGG decreased SA-β-Gal staining (Figure 3e,f) as well as the expression of p21 and increased expression of PCNA (Figure 3g,h) in presence of CQ in PC3 cells. Taken together, AGG induces autophagy in prostate cancer cells, which might be the prerequisite for TIS.

3.3 | AGG-induced lipophagy modulates senescence

Lipophagy refers to the autophagic degradation of LDs by the lysosomal acid lipase to FFAs. During nutrient depletion, the hydrolysis of LD-sequestered triglycerides (TGs) generates FFAs for replenishing cellular energy (Settembre & Ballabio, 2014). We hypothesized therefore that lipophagy plays an important role in AGG-induced senescence. PC3 cells were stained with LipidTOX™ Green to evaluate lipid degradation, and the number of LDs was significantly reduced in the AGG-treated cells compared with the untreated controls (Figure 4a,b). Interestingly, AGG-induced decrease in LDs was restored in the presence of CQ as compared with only AGG-treated group in PC3 cells (Figure 4a,b). Consistent with this, the levels of the LD protein perilipin 2 was significantly decreased in the AGG-treated cells (Figure 4c,d). In addition, AGG-treated PC3 cells showed a significant

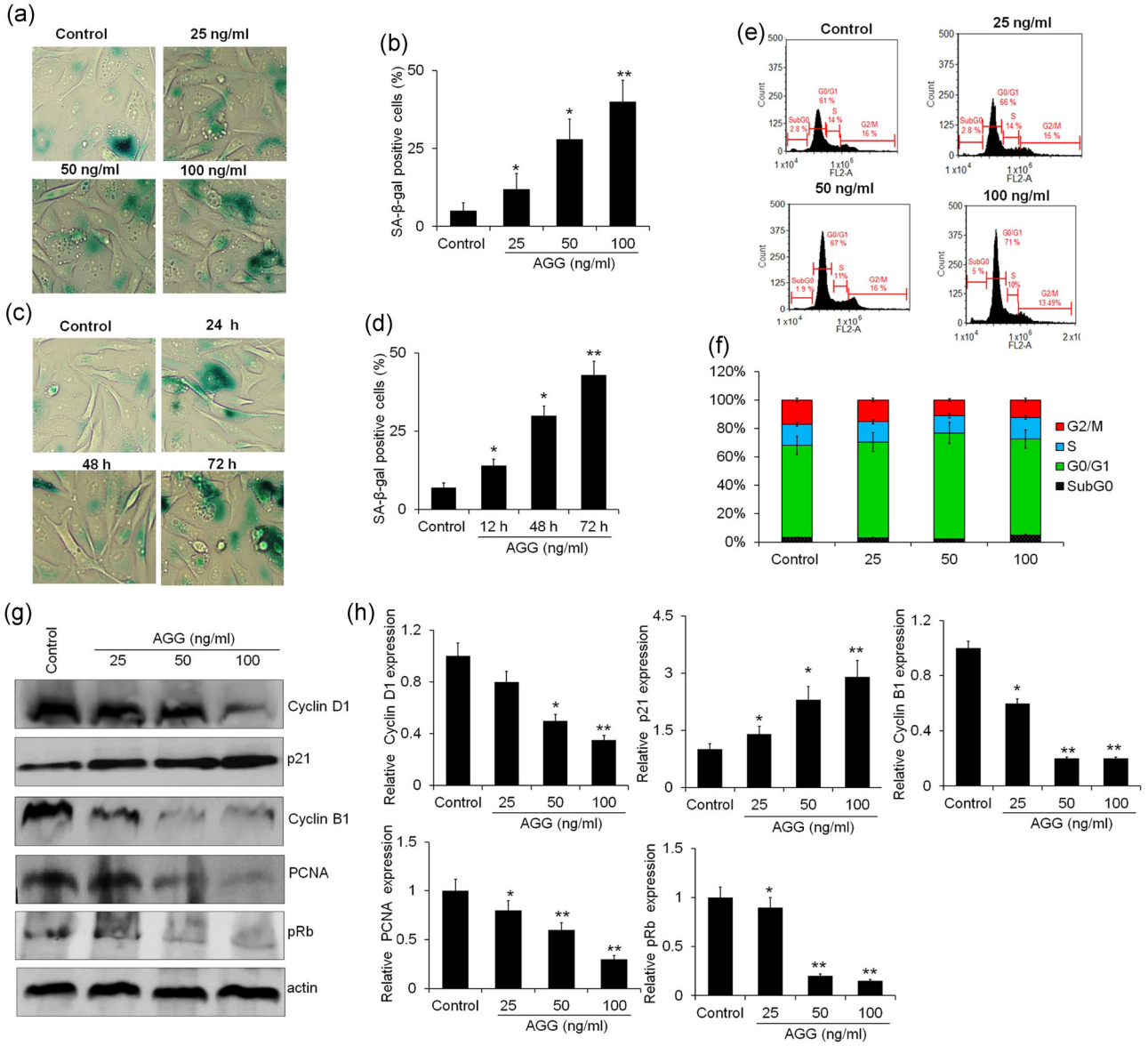

FIGURE 1 AGG induces therapy-induced senescence in PC3 cells: PC3 cells were treated with different doses of AGG (25, 50, and 100 ng/ml) at different times (24, 48, and 72 hr) and senescence was examined by SA-β-Gal staining through bright field microscopy (Olympus IX–71, 400×) (a–d) After treatment with AGG, PC3 cells were analyzed for cell cycle distribution by PI staining through flow cytometry (e, f) After 72 hr of AGG treatment, PC3 cells were analyzed for expression of p21, cyclin D1, pRb, cyclin B1, and PCNA by western blot analysis (g). The data reported as the mean ± *SD* of three independent experiments and compared with PBS control. The relative expression of proteins was quantified taking actin as the loading control (h). AGG, *Abrus* agglutinin; PBS, phosphate-buffered saline; PC3, prostate carcinoma cell line; PCNA, proliferating cell nuclear antigen; PI, propidium iodide. $^{*}p < .05$ and $^{**}p < .01$ were considered significant [Color figure can be viewed at wileyonlinelibrary.com]

colocalization of RFP-LC3 and LipidTox, which was indicative of lipophagy (Figure 4e,f). In addition, Oil Red O staining data in PC3 cells showed that there was a dose-dependent decrease in the number of Oil Red O-stained LDs with AGG treatment (Figure 5). The lipophagic ability of AGG was further displayed by a dose-dependent increase in the FFAs content (Figure 5).

To further validate our hypothesis, we pretreated the cells with lalistat, an inhibitor of lysosomal lipase and therefore of lipophagy, and found that it not only reversed AGG-induced degradation of LDs into FFAs (Figure 5), but also significantly reduced the percentage SA-β-Gal-positive cells (Figure 6a,b). In addition, the presence of lalistat also downregulated p21 and upregulated PCNA in the AGG-treated cells (Figure 6c,d). Finally, tracking the autophagy flux revealed a significant decrease in red fluorescent punctae in the AGG-lalistat co-treated cells compared with those treated only with AGG (Figure 6e,f) indicating AGG triggers lipophagy in PC3 cells leading to senescence.

3.4 | SIRT1 regulates AGG-induced autophagy and senescence

SIRT1 is associated with cellular processes like senescence, autophagy, and apoptosis (Chua et al., 2005; Fang & Nicholl, 2011). To determine

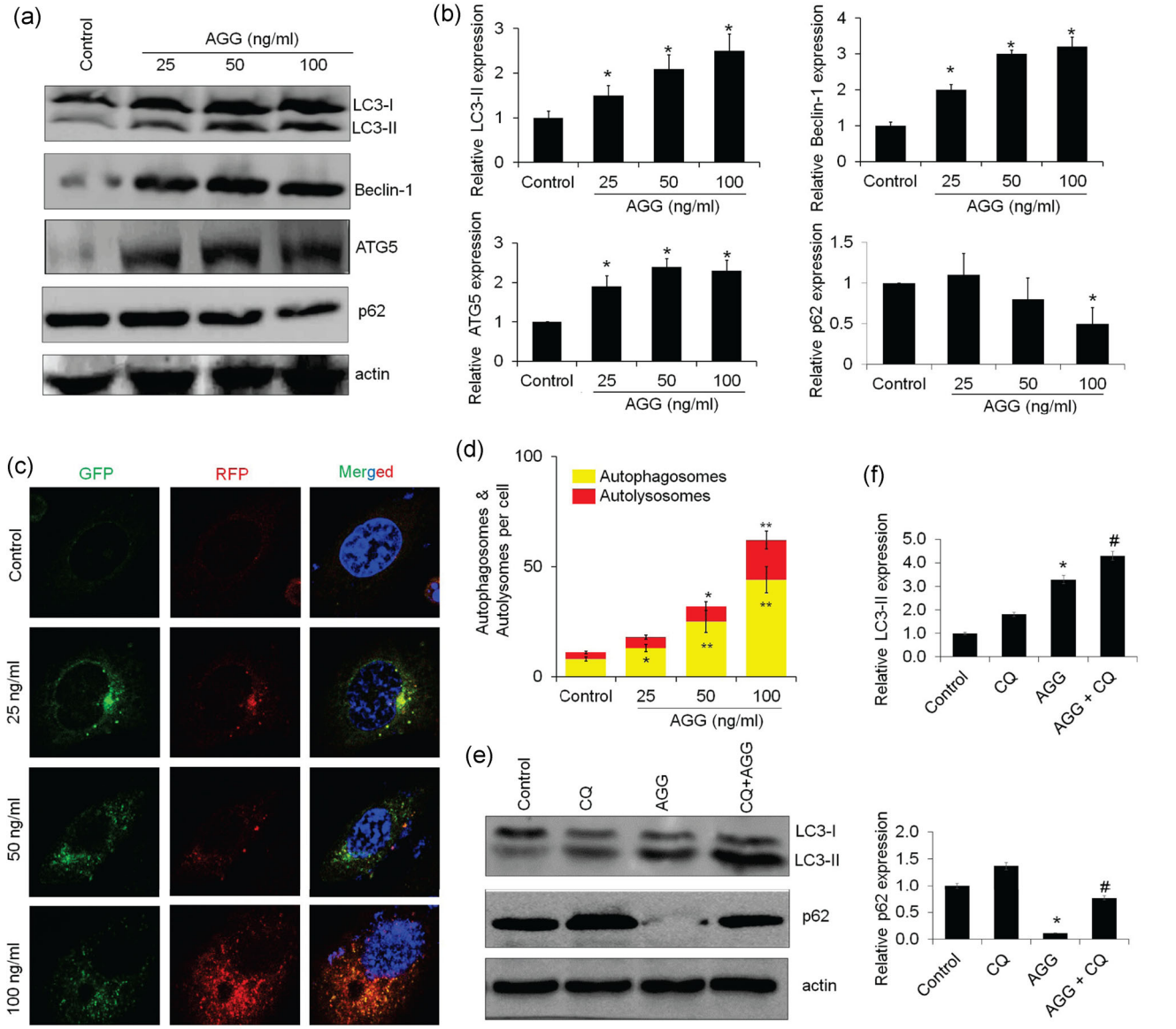

FIGURE 2 AGG promotes autophagy in PC3 cells. PC3 cells were treated with different doses (25, 50, and 100 ng/ml) of AGG for 72 hr and the expression of autophagic proteins was analyzed by western blot analysis (a). The relative expression of autophagic proteins was quantified taking actin as the loading control (b). The autophagic flux analysis in 72 hr AGG-treated PC3 cells was done after tfLC3 transfection, and the numbers of RFP + GFP + (yellow) and RFP + GFP− (red) puncta per cell represented autophagosome and autolysosome, respectively, and were quantified through confocal microscopy (Olympus FV−1000, ×630) (c, d). The autophagic flux was determined using CQ (40 μM, 2 hr) post-treatment with AGG (100 ng/ml) for 72 hr and the expression of LC3 and p62 was determined by western blot analysis (e). The relative expression of LC3 and p62 was quantified taking actin as the loading control (f). AGG, *Abrus* agglutinin; CQ, chloroquine; GFP, green fluorescent protein; PC3, prostate carcinoma cell line; RFP, red fluorescent protein; tfLC3, tandem fluorescent-tagged. $^{*}p < .05$ and $^{**}p < .01$ were considered significant as compared to control. $^{\#}p < .05$ was considered significant in comparison to AGG-treated group [Color figure can be viewed at wileyonlinelibrary.com]

whether SIRT1 is also involved in AGG-induced autophagy, we first analyzed the expression levels of SIRT1 in the AGG-treated cells and found that AGG upregulated SIRT1 in PC3 cells in a dose-dependent manner (Figure 7a–d). Furthermore, inhibiting SIRT1 activity with its specific inhibitor sirtinol resulted in a significant reduction in AGG-induced SA-β-Gal staining (Figure 7e,f) and p21 expression increased expression of PCNA (Figure 7g,h), and decreased autophagy flux (Figure 7i,j) compared with the only AGG-treated cells. These findings indicate that SIRT1 plays a pivotal role in AGG-induced autophagy/lipophagy and senescence in PC3 cells.

3.5 | AGG-induced SIRT1 deacetylates LAMP1 to induce autophagy/lipophagy

Although SIRT1 lies initially in the nucleus but it shuttles between nucleus and cytoplasm which depends upon the various stimuli

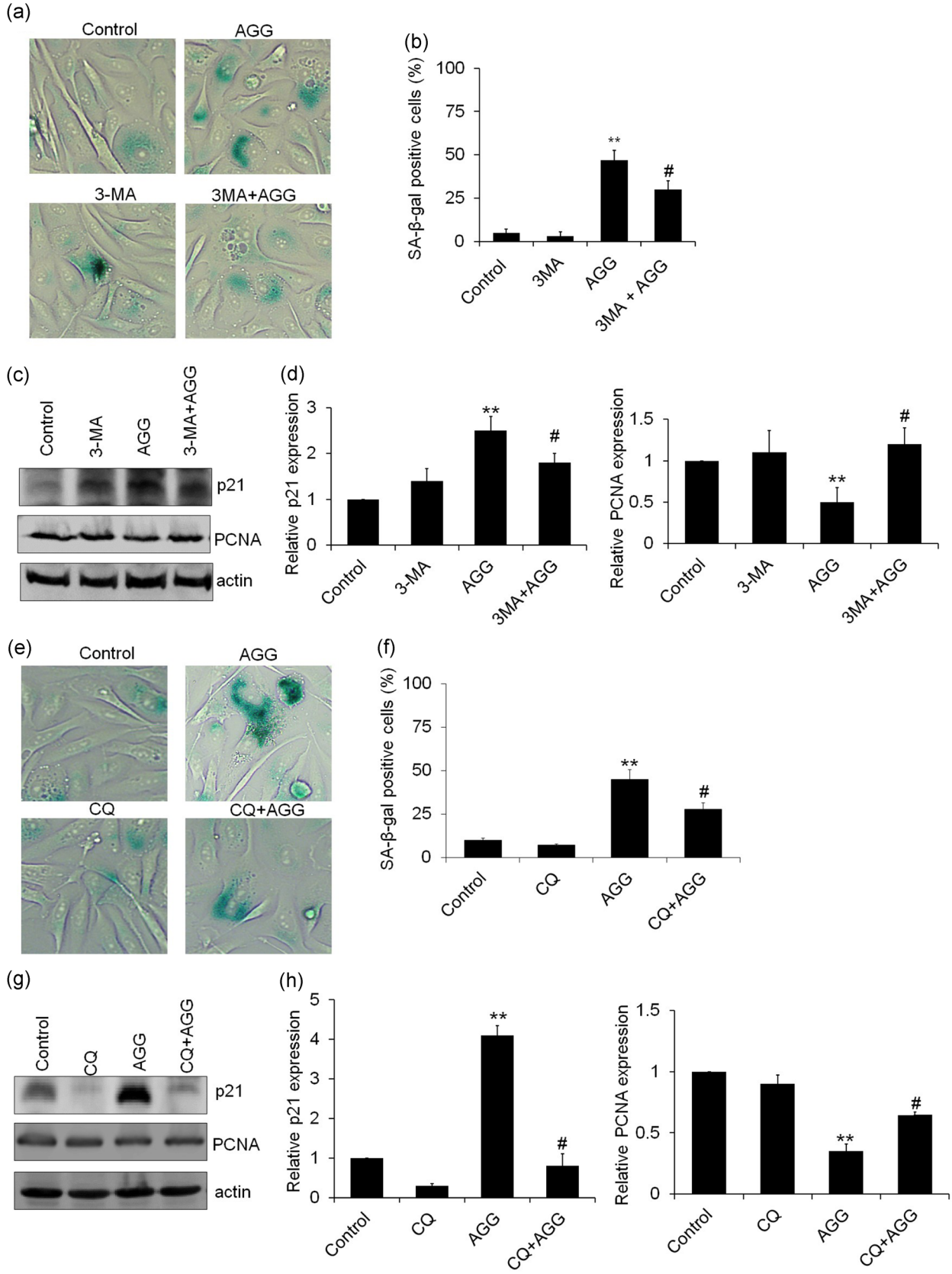

FIGURE 3 Continued.

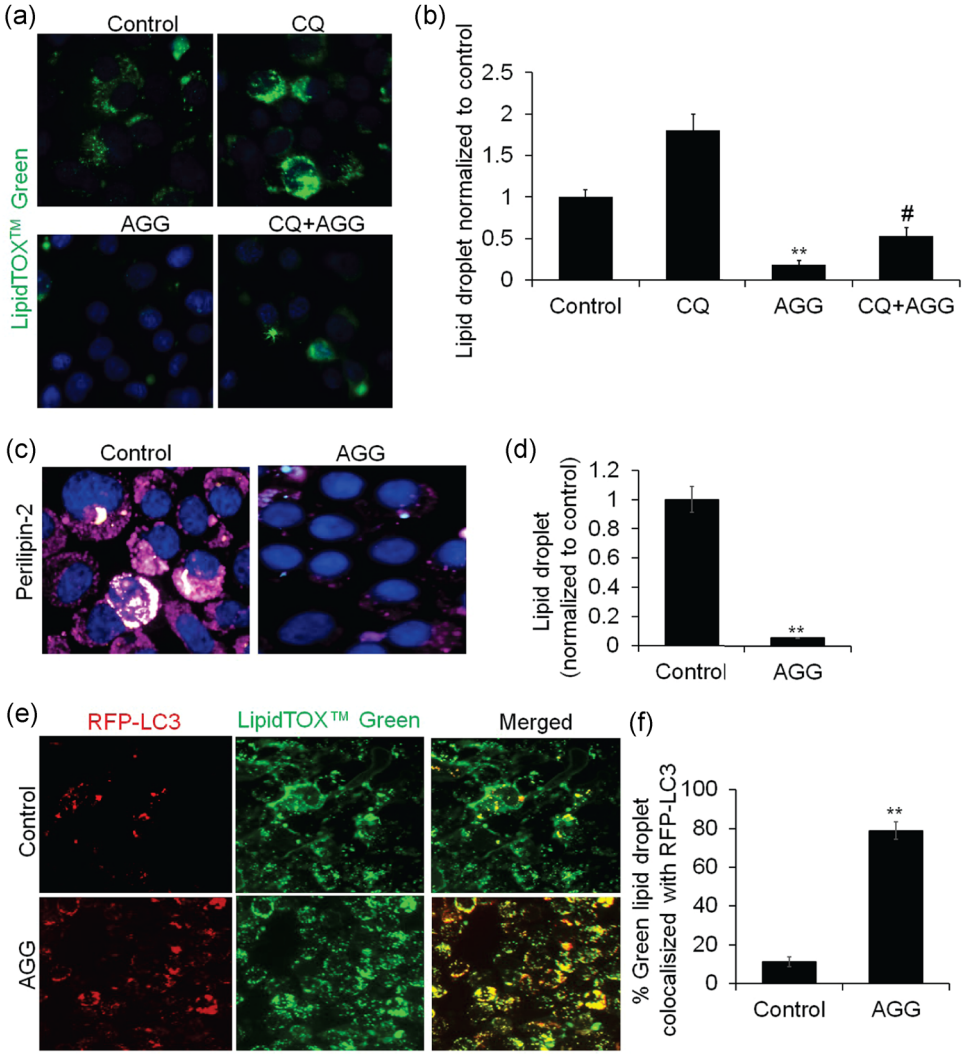

FIGURE 4 AGG triggers lipophagy in PC3 cells. PC3 cells were treated with AGG (100 ng/ml) for 72 hr in presence of CQ (40 μM, 2 hr) and lipid droplet staining was performed using LipidTOX™ Green (1 μM, 30 min) (a, b) through confocal microscopy. The droplet-associated protein Perilipin 2 (PLIN2) was quantified after 72 hr AGG treatment through confocal microscopy (c, d). PC3 cells were transfected with RFP-LC3 and stained with PLIN2 after 72 hr AGG (100 ng/ml) treatment and interaction of LC3 and PLIN2 were analyzed through confocal microscopy (e, f). The data reported as the mean ± *SD* of three independent experiments and compared with PBS control. AGG, *Abrus* agglutinin; CQ, chloroquine; PBS, phosphate-buffered saline; PC3, prostate carcinoma cell line; PLIN2, Perilipin 2; RFP, red fluorescent protein. $^{**}p < .01$ was considered significant. $^{\#}p < .05$ was considered significant as compared with the AGG-treated group [Color figure can be viewed at wileyonlinelibrary.com]

(Gewirtz, 2013). Accumulating evidence indicates that SIRT1 present principally in the cytoplasm of cancer as well as transformed cells to maintain PI3K-directed cancer cell growth (Byles et al., 2010). The analysis of the cellular and nuclear protein fractions of PC3 cells indicated SIRT1 localization in the cytoplasm of PC3 cells (Figure 8a). Interestingly, SIRT1 has been found to regulate basal autophagy through deacetylation of nuclear LC3 at K49 and K51 during starvation. In this setting, AGG-treated cells had increased levels of deacetylated LAMP1 compared with the untreated cells (Figure 8b). Based on these findings, we hypothesized that AGG induced

FIGURE 3 AGG-induced autophagy regulates senescence in PC3 cells. PC3 cells were treated with AGG (100 ng/ml) for 72 hr in the presence of 3-MA (10 mM, 2 hr) and senescence was examined by SA-β–Gal staining (a and b) and western blot analysis (c). The relative expression of p21 and PCNA was quantified taking actin as the loading control (d). PC3 cells were treated with AGG (100 ng/ml) for 72 hr in the presence of CQ (40 μM, 2 hr) and senescence was examined by SA-β–Gal staining (e and f) and western blot analysis (g). The relative expression of p21 and PCNA was quantified taking actin as the loading control (h). AGG, *Abrus* agglutinin; CQ, chloroquine; PC3, prostate carcinoma cell line; PCNA, proliferating cell nuclear antigen; 3-MA, 3-methyl adenine. $^{**}p < .01$ was considered significant. $^{\#}p < .05$ was considered significant as compared with the AGG-treated group [Color figure can be viewed at wileyonlinelibrary.com]

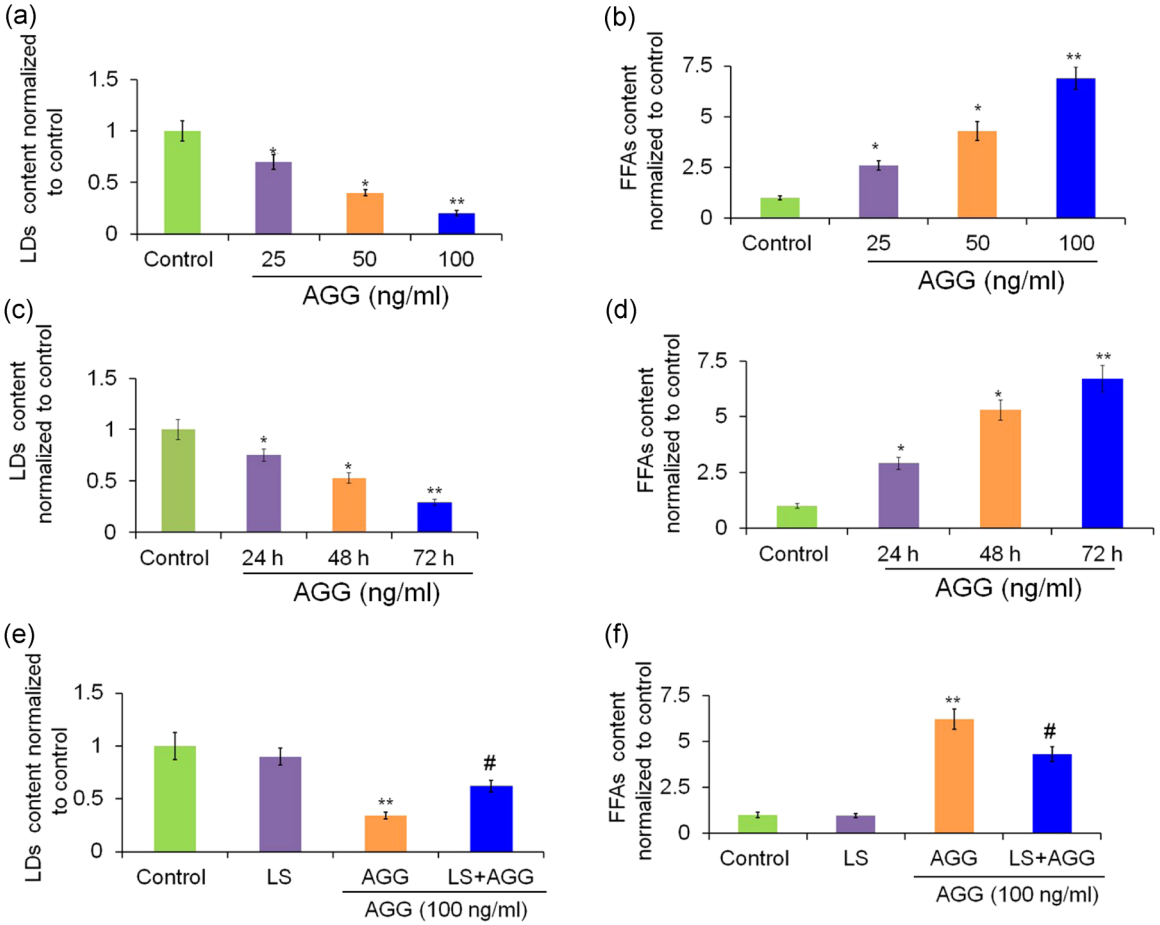

FIGURE 5 AGG regulates the content of lipid droplet and free fatty acid in PC3 cells. PC3 cells were treated with AGG for different doses (25, 50, and 100 ng/ml) and time periods and the relative contents of lipid droplets and free fatty acids were analyzed and quantified (a-d). PC3 cells were treated with AGG (100 ng/ml) in the presence of lalistat (10 μM, 6 hr) and the relative contents of lipid droplets and free fatty acids were measured (e, f). Data reported as the mean ± *SD* of three independent experiments and compared against PBS control. AGG, *Abrus* agglutinin; PBS, phosphate-buffered saline; PC3, prostate carcinoma cell line. $^{*}p < .05$; $^{**}p < .01$ were considered significant. $^{\#}p < .05$ was considered significant as compared with the AGG-treated group [Color figure can be viewed at wileyonlinelibrary.com]

autophagy in PC3 cells via SIRT1-mediated LAMP1 deacetylation. This hypothesis was first supported by the co-immunoprecipitation of SIRT1 and LAMP1 in AGG-treated PC3 lysates (Figure 8c), which indicates a direct physical interaction between the two proteins.

To identify the residues of the individual SIRT1 and LAMP1 domains involved in their interactions, a 20-ns long MD simulation of the docked SIRT1–LAMP1 complex was performed. LAMP1 is a 417-amino acid long having highly glycosylated end with N-linked carbon chains on the luminal side (29–382), transmembrane domain (383–405). across lysosomal membranes, and a short C-terminal tail (406–417) exposed to the cytoplasm (Eskelinen, 2006; Figure 8d). As shown in Figure S1, the model was stable with Cα atoms root mean square deviations value of 2–5 Å. Our data showed that the C-terminal part of LAMP1 putatively binds to the active site of SIRT1 at Lys 408, resulting in its deacetylation. MM-GBSA-based average binding free energy and the detailed contributions from various energy components were calculated for SIRT1–LAMP1 complex by taking 500 snapshots from the 11–20 ns of the MD trajectory (Figure 8e). As shown in Table S1, the calculated binding free energy was −33.889 kcal/mol, with electrostatic interactions contributing the most at −431.174 kcal/mol. However, the favorable contribution from the direct electrostatic interactions between SIRT1 and LAMP1 was recompensed by the electrostatic desolvation free energy upon binding, which progressed to an unfavorable contribution as a whole, consistent with other MM-GBSA and MM-PBSA studies. In contrast, nonpolar interactions, $\Delta G_{nonpolar}$ (including van der Waals interactions and nonpolar solvation) contributed − 113.054 kcal/mol, which is very favorable to the binding process and consistent with the large hydrophobic binding surface between SIRT1 and LAMP1 (Figure 8f). Therefore, we concluded that the binding of SIRT1 and LAMP1 was largely via nonpolar interactions like van der Waals interactions and the nonpolar solvation contribution. Several residues of LAMP1—Thr230, Asn261, Ile401, Leu404, Val405, Arg409, and Ile417—favorably contributed >−2.0 kcal/mol. In addition, other residues (including Ala265 and Tyr414) contributed >−1.0 kcal/mol, while Asn1 counteracted the binding by contributing an unfavorable ΔG of >+3.20 kcal/mol (Figure 8g). The residue energy decomposition results for SIRT1 showed that Asp277,

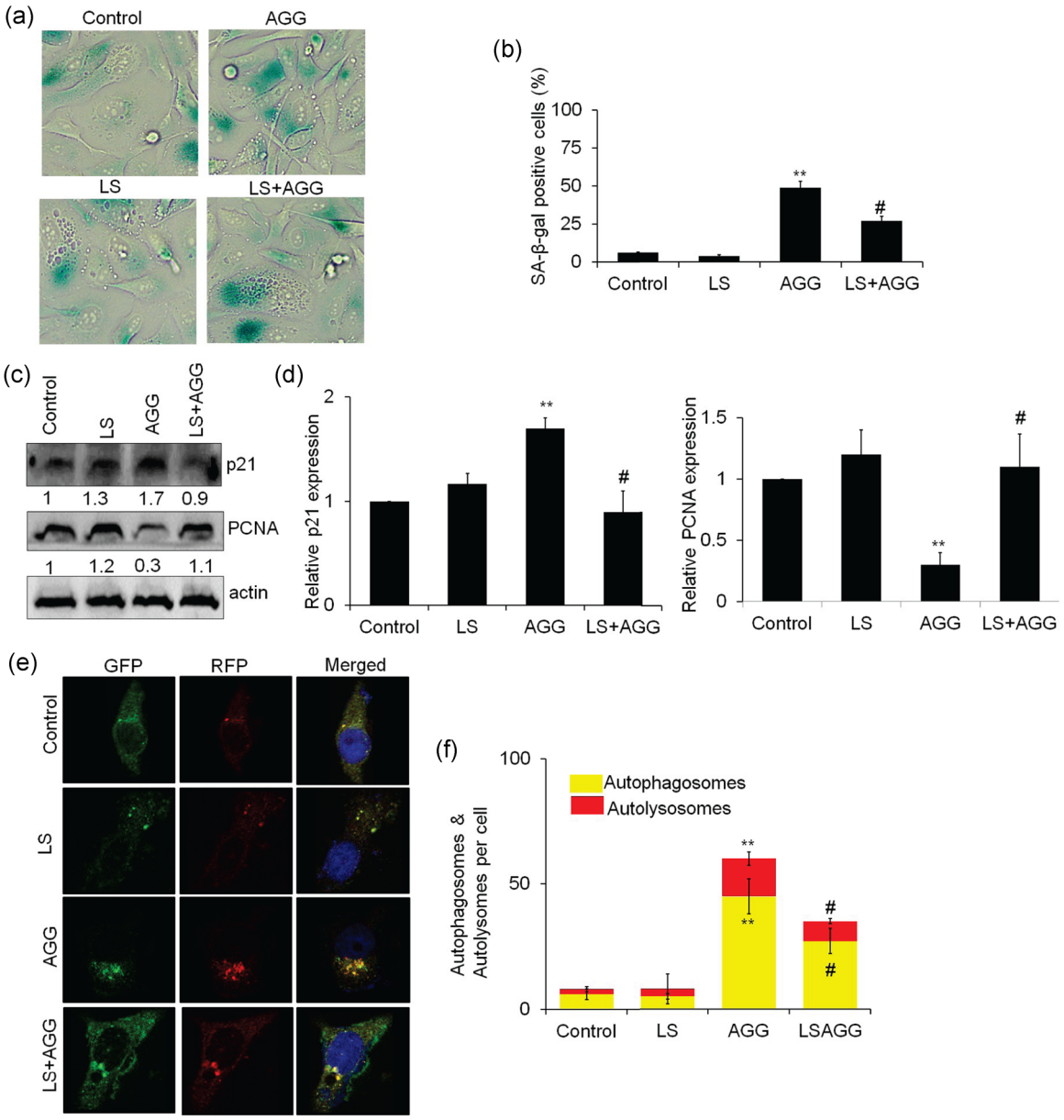

FIGURE 6 AGG induces lipophagy to prompt senescence in PC3 cells. PC3 cells were treated with AGG (100 ng/ml) for 72 hr in the presence of lalistat (10 μM, 6 hr) and senescence was examined SA-β–Gal staining (a, b) and western blot analysis (c). The relative expression of p21 and PCNA was quantified taking actin as the loading control (d). After AGG (100 ng/ml) treatment in the presence of lalistat (10 μM, 6 hr), the autophagic flux in tfLC3 was quantified through confocal microscopy (e, f). Data reported as the mean ± *SD* of three independent experiments and compared with PBS control. AGG, *Abrus* agglutinin; PBS, phosphate-buffered saline; PC3, prostate carcinoma cell line; PCNA, proliferating cell nuclear antigen. $^{**}p < .01$ was considered significant as compared with control and $^{\#}p < .05$ was considered significant as compared with the AGG-treated group [Color figure can be viewed at wileyonlinelibrary.com]

Phe388, Gln390, and Arg446 in SIRT1 each contributed >−2.0 kcal/mol, while Pro271, Asp272, Ser275, Val285, and His471 contributed ≥−1.0 kcal/mol of the free energy and Arg276, Lys311, and Lys314 counteracted the binding by contributing unfavorable ΔG of > +1.0 kcal/mol (Figure 8h). These residues are present on the SIRT1 surface on one of the α-helices in the middle region and form a part of the active site. The chief contributors for the binding, that is Asp277, Phe388, and Arg446, are present in different regions but Asp277 and Arg446 form a part of the SIRT1 active site.

3.6 | Lipophagy-dependent FFA accumulation by AGG promotes reactive oxygen species to influence senescence

Cellular FFA stimulates ROS generation and mediates ROS-induced apoptosis, autophagy, and senescence (Mukhopadhyay et al., 2017; Schonfeld & Wojtczak, 2008; Settembre & Ballabio, 2014). In our previous study, we showed that AGG triggers ROS generation to initiate apoptosis and autophagy in cancer cells as a

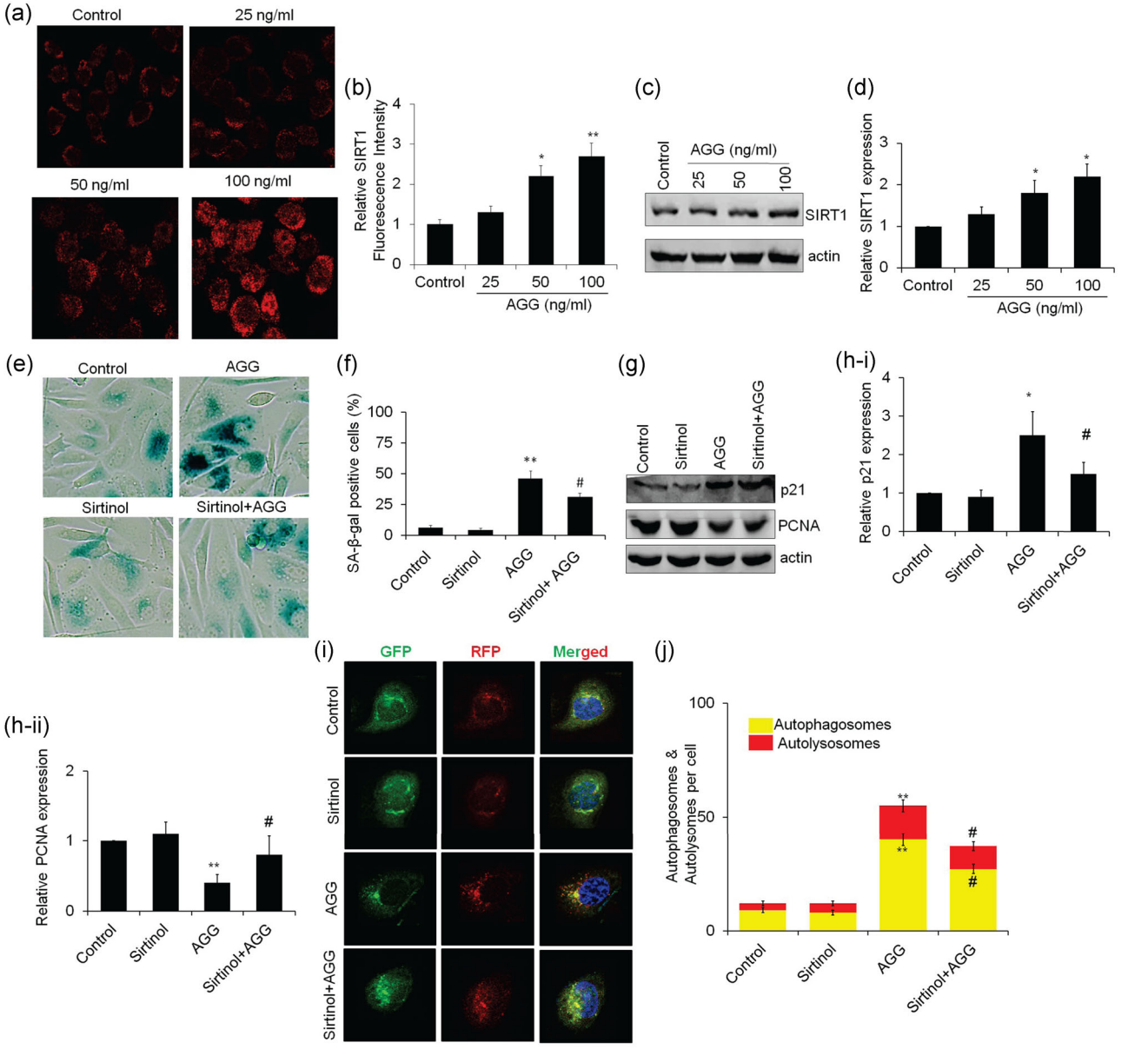

FIGURE 7 SIRT1 regulates AGG-induced senescence in PC3 cells. PC3 cells were treated with different doses of AGG (25, 50, and 100 ng/ml) and SIRT1 expression was analyzed through confocal microscopy (a, b) and western blot (c). The relative expression of SIRT1 was quantified taking actin as the loading control (d). PC3 cells were treated with AGG (100 ng/mL) in the presence of sirtinol (5 μM, 2 hr) and senescence was examined SA-β–Gal staining (e,f) and western blot analysis (g). The relative expression of p21 and PCNA was quantified taking actin as the loading control (h). After AGG (100 ng/ml) treatment in the presence of sirtinol (5 μM, 2 hr), the autophagic flux in tfLC3 was quantified through confocal microscopy (i, j). Data reported as the mean ± *SD* of three independent experiments and compared with PBS control. AGG, *Abrus* agglutinin; PBS, phosphate-buffered saline; PC3, prostate carcinoma cell line; SIRT1, silent mating type information regulation 1; tfLC3, tandem fluorescent-tagged. $^{*}p < .05$; $^{**}p < .01$ were considered significant as compared with control and $^{\#}p < .05$ was considered significant as compared to AGG-treated group [Color figure can be viewed at wileyonlinelibrary.com]

tumor-suppressive mechanism. To determine the role of ROS in AGG-induced senescence, we pretreated PC3 cells with the ROS scavenger *N*-acetyl cysteine followed the treatment of AGG, and found a significant depletion in SA-β–Gal-positive senescent cells compared with the only AGG-treated cells (Figure 9a,b). Furthermore, AGG-induced ROS accumulation declined significantly in the presence of lalistat (Figure 9c). Taken together, AGG-induced FFAs promote ROS generation to stimulate senescence in PC3 cells.

4 | DISCUSSION

Therapy induced senescence refers to a permanent cytostatic condition in cancer cells because of anti-neoplastic drugs or radiation (Gewirtz, 2013; Gewirtz et al., 2008; Vargas et al., 2012). Studies show that phytochemicals, such as resveratrol (Patel et al., 2013), punicalagin (Cheng et al., 2018), thymoquinone (Subburayan, Thayyullathil, Pallichankandy, Rahman, & Galadari, 2018), and bufalin

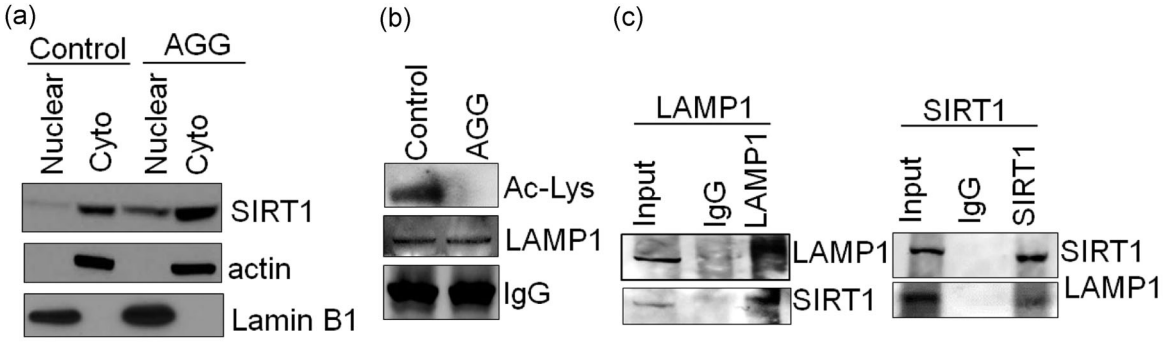

(d)

Human LAMP1

MAAPGSARRPLLLLLLLLLLGLMHCASAAMFMVKNGNGTACIMANFSAAFSVNYDTKSGPKNMTFDLPSD
29
ATVVLNRSSCGKENTSDPSLVIAFGRGHTLTLNFTRNATRYSVQLMSFVYNLSDTHLFPNASSKEIKTVE
SITDIRADIDKKYRCVSGTQVHMNNVTVTLHDATIQAYLSNSSFSRGETRCEQDRPSPTTAPPAPPSPSP
SPVPKSPSVDKYNVSGTNGTCLLASMGLQLNLTYERKDNTTVTRLLNINPNKTSASGSCGAHLVTLELHS
EGTTVLLFQFGMNASSSRFFLQGIQLNTILPDARDPAFKAANGSLRALQATVGNSYKCNAEEHVRVTKAF
SVNIFKVWVQAFKVEGGQFGSVEECLLDENSM LIPIAVGGALAGLVLIVLIAYLV GRKRSHAGYQTI
Luminal 382 383 **Transmembrane** 405 406 **Cytoplasmic** 417

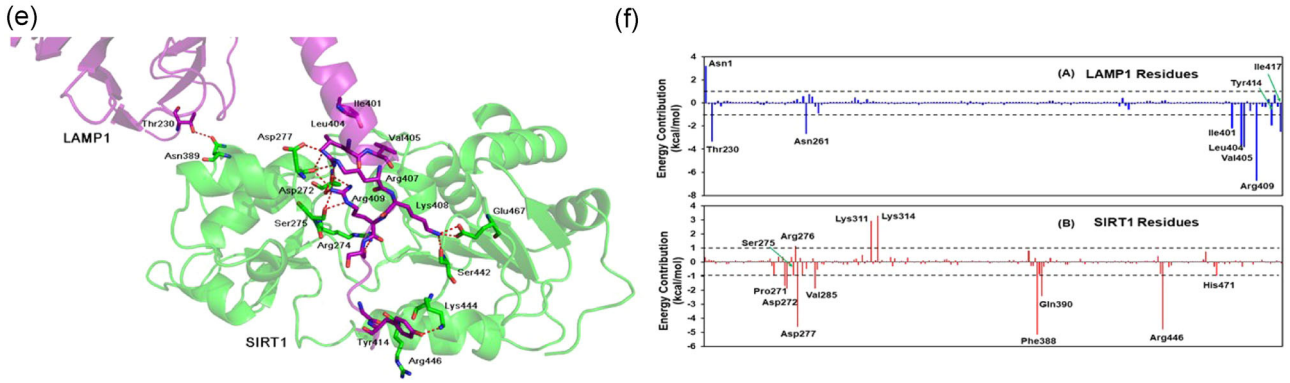

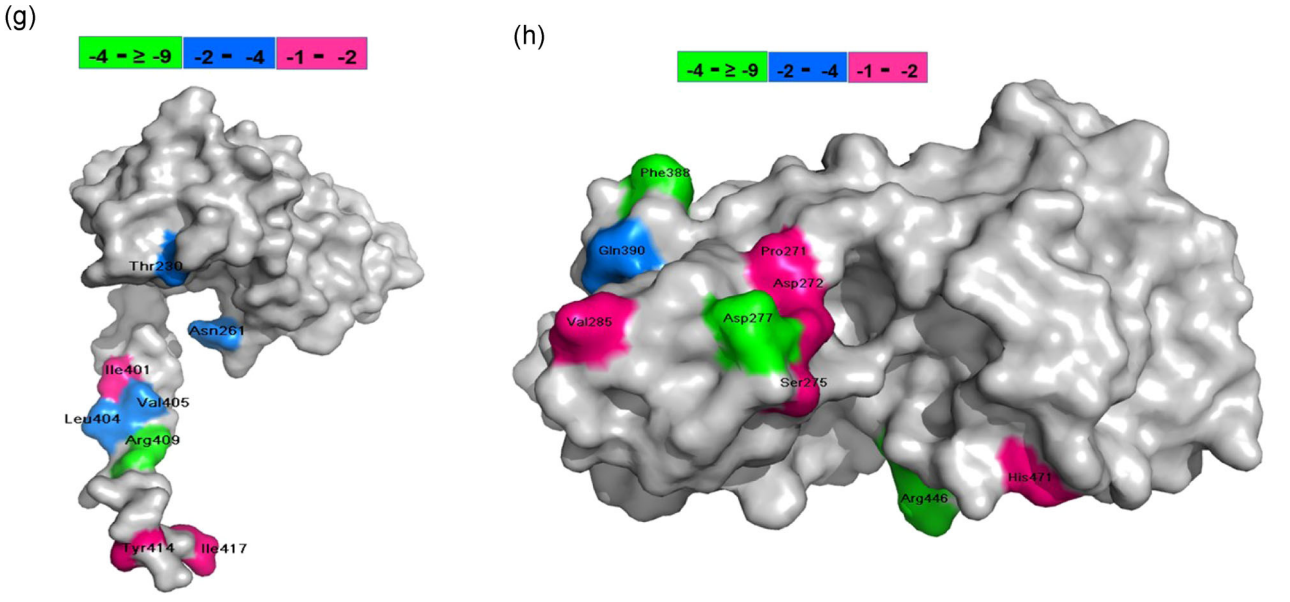

FIGURE 8 Continued.

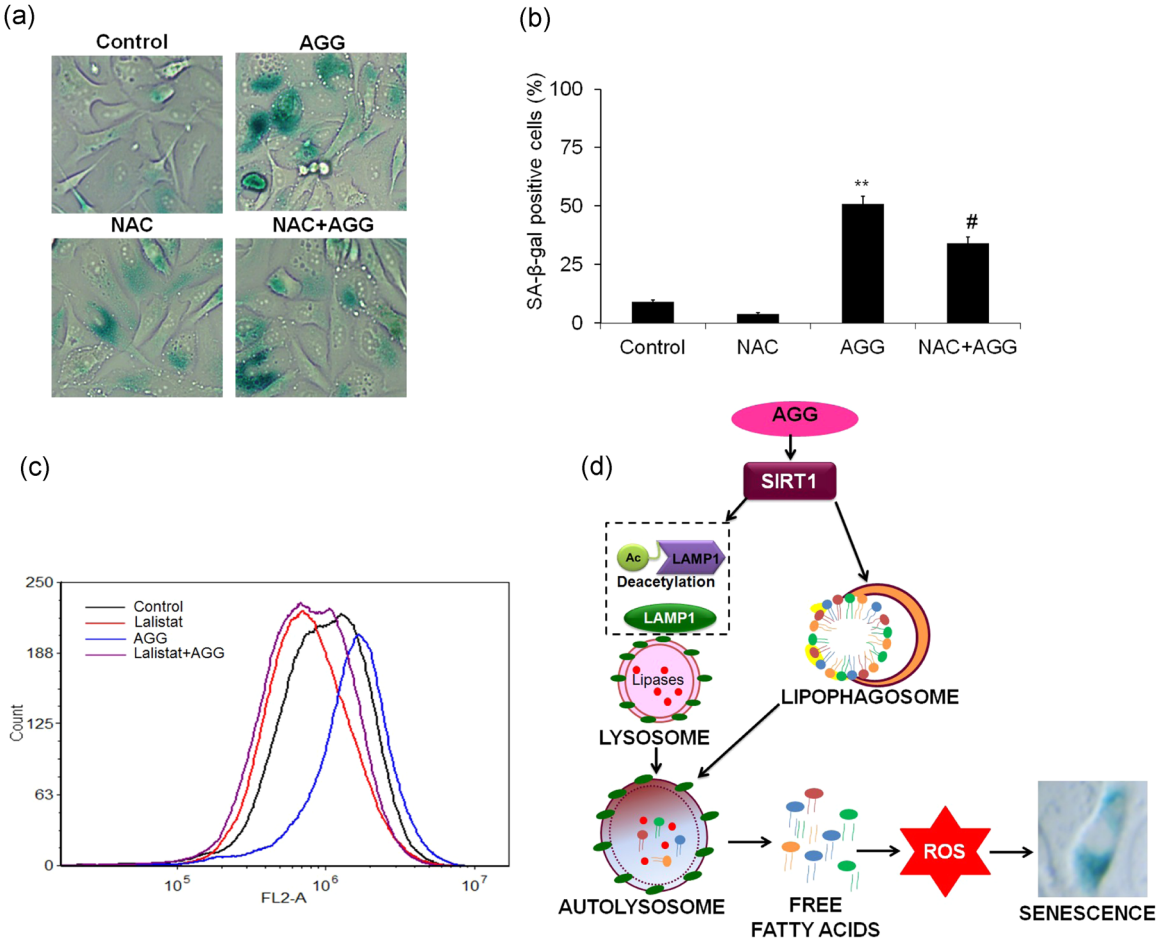

FIGURE 9 AGG-induced ROS through lipophagy inflicts senescence in PC3 cells. PC3 cells were treated with AGG (100 ng/ml) in the presence of NAC (5 mM, 2 hr) and senescence was examined SA-β–Gal staining (a, b). After AGG (100 ng/ml) treatment in the presence of lalistat (10 μM, 6 hr), ROS generation was quantified through flow cytometry (c). $^{**}p < .01$ were considered significant as compared with control and $^{\#}p < .05$ was considered significant as compared with the AGG-treated group. A schematic representation depicting the mechanism of AGG inducing senescence through lipophagy in PC3 cells (d). AGG, *Abrus* agglutinin; NAC, *N*-acetylcysteine; PC3, prostate carcinoma cell line [Color figure can be viewed at wileyonlinelibrary.com]

(Y. Zhang et al., 2018) can effectively promote an indefinite growth arrest of cancer cells by inducing a senescence-like phenotype. In our previous study, we found that peanut agglutinin induced senescence in tumor cells at low doses, along with apoptosis and autophagy (Mukhopadhyay, Panda, Behera et al., 2014). In addition, several studies have established that the process of senescence is linked to autophagy (Fang & Nicholl, 2011; Gewirtz, 2013; Goehe et al., 2012). Previously, we have reported the autophagy inducing potential of AGG (Panda et al., 2017; Panda, Naik, Meher, et al., 2018; Panda, Naik, Praharaj, et al., 2018), therefore in the present study, we investigated the pro-senescent activity of AGG on prostate carcinoma cells and its underlying mechanisms. Low doses of AGG induced

FIGURE 8 AGG-induced SIRT1 deacetylates LAMP1 to induce autophagy/lipophagy in PC3 cells. Cytoplasmic and nuclear fractions of PC3 cells were isolated, the same amount of nuclear and cytoplasmic protein was subjected to SDS gel, and immunoblots were performed with anti-SIRT1, actin and LaminB1 antibodies (a). After treatment with AGG (100 ng/ml), the acetylation of LAMP1 in PC3 cells was studied by immunoprecipitation analysis (b). PC3 cells were treated with AGG (100 ng/ml) for 72 hr and immunoprecipitated with anti-SIRT1 and anti-LAMP1 followed by immunoblotting with anti-LAMP1 or anti-SIRT1 antibodies (c). The sequence of LAMP1 with different domain luminal side (blue), transmembrane domain (pink) and cytoplasmic tail (red) (d). A schematic ribbon representation of the docked SIRT1–LAMP1 complex structure is shown in different colors. The SIRT1 domain is shown in green color while the LAMP1 structure is shown in violet color. Residues showing the interactions are shown as sticks along the domain interface for both SIRT1 and LAMP1 (e). The decomposition of ΔG on a per-residue basis or the pair interaction energy between SIRT1 and LAMP1: (a) the contribution of each residue in LAMP1 to SIRT1 binding; (b) the contribution of each residue in the SIRT1 domain to LAMP1 binding (f). The distributions of the identified hotspot residues on the SIRT1 (g) and LAMP1 (h) domain cartoon representation. Colored bars show the range of contributions by the residues in the unit kcal/mol. AGG, *Abrus* agglutinin; LAMP1, lysosome-associated membrane protein 1; PC3, prostate carcinoma cell line; SDS, sodium dodecyl sulfate; SIRT1, silent mating type information regulator 2 homolog 1 [Color figure can be viewed at wileyonlinelibrary.com]

autophagy-dependent senescence in the prostate cancer cells, specifically via lipophagy and FFAs (Figure 9d).

TIS has been reported in cancer cells following exposure to various cytotoxic agents both in vitro and in vivo (Gewirtz, 2013). AGG-treated PC3 cells showed a robust dose-dependent increase in SA-β-Gal staining, indicating senescence. Unlike apoptotic cells or those that undergo mitotic catastrophe, senescent cells persist indefinitely. Growth arrest in the senescent cells at G1 or G2/M stages of the cell cycle occurs in part via the upregulation of specific CDKIs, including p16Ink4a (CDKN2A), p21Waf1 (CDKN1A/CIP1), and p27Kip1 (CDKN1B) (Gewirtz et al., 2008; Patel et al., 2013). Accordingly, AGG induced cell cycle arrest at the G1 phase and upregulated p21, downregulated cyclins D1 and B1 and the proliferation marker PCNA, and hypo-phosphorylated the tumor suppressor Rb to accelerate senescence. Senescence associated genes p21 and p16 are likely to modulate the phosphorylation status of pRb during senescence either by permanently inactivation or through prolonged hypo-phosphorylation (Dimri, 2005). Therefore, unlike apoptosis, senescence requires much lower doses of AGG, which is favorable in the clinical setting.

Radiation or chemotherapy-induced autophagy is often required for activating senescence (Gewirtz, 2013; Goehe et al., 2012). For example, ionizing radiation promoted senescence in PTTG1/securin deficient breast cancer cells via autophagy to suppress proliferation (Y. H. Huang et al., 2014). Interestingly, several phytochemicals like resveratrol (Patel et al., 2013), *Rhus coriaria* extract (El Hasasna et al., 2015) and pseudolaric acid B (Qi et al., 2013) among others can induce both autophagy and senescence in human cancer cells. Accordingly, inhibition of pseudolaric acid B induced autophagy abrogated the senescent phenotype in L929 cells (Qi et al., 2013), further underscoring that autophagy facilitates senescence. In our study also, AGG was unable to induce SA-β-Gal expression in prostate cancer cells in the presence of 3-MA, thereby confirming that autophagy precedes senescence in response to AGG exposure. To determine the underlying mechanism, we analyzed alterations in lipid metabolism and found that AGG induced lipophagy, a selective autophagic-lipolytic pathway that generates FFAs, which triggered senescence in the PC3 cells. FFAs are known to activate mitochondrial β-oxidation (Schonfeld & Wojtczak, 2008) and autophagy-induced FFAs drive neutrophil differentiation via the mitochondrial metabolic pathway (Riffelmacher et al., 2017). In a recent study, we found that lipophagy in cancer cells induced ER stress-mediated apoptosis (Mukhopadhyay et al., 2017). In the present study, AGG-induced FFA accumulation through lipophagy increased ROS generation, which in turn activated senescence; furthermore, inhibition of lipophagy by lalistat reduced the percentage of senescent cells, thus confirming the causative role of FFAs in senescence.

SIRT1 is a key regulator in both stress-induced autophagy and senescence (Chua et al., 2005; R. Huang et al., 2015). A previous study reported that SIRT1 triggered senescence and cell cycle arrest in human colorectal carcinoma cells in response to chronic genotoxic stress via a p19 and p53 dependent pathway (Chua et al., 2005) and SIRT1 knockdown reversed the senescent phenotype in aspirin-treated cells (Jung et al., 2015). Consistent with this, we found that AGG upregulated SIRT1 in PC3 cells to induce senescence, which was abrogated by sirtinol-mediated inhibition of SIRT1. Moreover, ER stress leads to activation of SIRT1 and we previously reported that AGG induces ER stress to positively regulate autophagy and apoptosis (Panda et al., 2017). In this connection, it is tempting to speculate that AGG could promote SIRT1 activation through ER stress-dependent pathway to induce senescence (Koga et al., 2015). Similarly, SIRT1 activation by resveratrol-induced autophagy and inhibited the growth of prostate cancer by inhibiting the S6K signaling pathway (G. Li et al., 2013). Recently, a novel small molecule activator of SIRT1 was shown to activate autophagy-dependent cell death in glioblastoma cells (Yao et al., 2018). Our findings also indicated that the induction of autophagy in the AGG-treated cells was dependent on SIRT1 activation, and pretreatment with sirtinol significantly reduced the autophagy flux in these cells. Deacetylation of lysine residues by SIRT1 is critical for the stability, activity and subcellular localization of various proteins, including those involved in autophagy. SIRT1-mediated deacetylation of nuclear LC3 at Lys49 and Lys51 causes the latter is translocation to the cytoplasm, where it induces autophagy during serum starvation (R. Huang et al., 2015). In addition, a recent study demonstrated that the flavonoid galangin induces autophagy through SIRT1-mediated deacetylation of LC3 in HepG2 cells (X. Li et al., 2016). We found that AGG-induced cytoplasmic SIRT1 deacetylated a Lys residue in the cytoplasmic domain of LAMP1, which directly led to lipophagy and senescence. However, the exact mechanism linking LAMP1 deacetylation to lipophagy, and thus senescence, is unknown. Our hypothesis is that the LDs containing lipophagosomes fuse with deacetylated LAMP1 to generate FFAs, which then trigger the downstream senescent pathway. In conclusion, the present study reveals a hitherto unknown function of SIRT1 as a potent autophagy/lipophagy inducer through LAMP1 deacetylation, which mediated AGG-dependent senescence in cancer cells (Figure 8d). In addition, our findings also present a novel function of lipophagy in contributing to TIS, which can be harnessed to improve therapeutic regimens in prostate cancer.

ACKNOWLEDGMENTS

Research support was partly provided by the Science and Engineering Research Board (SERB) (number: EMR/2016/001246), Department of Science and Technology; Council of Scientific and Industrial Research (CSIR), (number: 37(1715)/18/EMR-II), Human Resource Development Group. Research infrastructure was partly provided by Fund for Improvement of S&T infrastructure in Universities & Higher Educational Institutions (FIST) (number: SR/FST/LSI-025/2014), Department of Science and Technology, Government of India. Authors sincerely thank Sushanta Pradhan for assisting in the confocal facility for this study work.

CONFLICT OF INTERESTS

The authors declare that there is no conflict of interests.

AUTHOR CONTRIBUTIONS

All authors were involved in drafting the article and critically revising important intellectual content. Conception: S.K.B., P.K.P., and P.P.P; study design: S.K.B., P.K.P., P.P.N., P.P.P., and S.P.; data acquisition: P.K.P., S.P., P.P.N., P.P.P., S.M., B.R.M., and P.K.G.; data analysis: S.K.B, P.K.P., B.R.M., T.K.M., and R.S.V.; data interpretation: S.K.B, P.K.P, P.P.P., S.P., B.R.M., T.K.M., and R.S.V. All authors approved the final version to be published.

DATA AVAILABILITY STATEMENT

The data that support the findings of this study are available from the corresponding author upon reasonable request.

ORCID

Sujit K. Bhutia http://orcid.org/0000-0003-0962-3354

REFERENCES

Bagaria, A., Surendranath, K., Ramagopal, U. A., Ramakumar, S., & Karande, A. A. (2006). Structure-function analysis and insights into the reduced toxicity of *Abrus precatorius* agglutinin I in relation to abrin. *Journal of Biological Chemistry*, *281*(45), 34465–34474. https://doi.org/10.1074/jbc.M601777200

Barnoud, T., Schmidt, M. L., Donninger, H., & Clark, G. J. (2017). The role of the NORE1A tumor suppressor in oncogene-induced senescence. *Cancer Letters*, *400*, 30–36. https://doi.org/10.1016/j.canlet.2017.04.030

Bhutia, S. K., Mallick, S. K., & Maiti, T. K. (2009). In vitro immunostimulatory properties of *Abrus lectins* derived peptides in tumor bearing mice. *Phytomedicine*, *16*(8), 776–782. https://doi.org/10.1016/j.phymed.2009.01.006

Byles, V., Chmilewski, L. K., Wang, J., Zhu, L., Forman, L. W., Faller, D. V., & Dai, Y. (2010). Aberrant cytoplasm localization and protein stability of SIRT1 is regulated by PI3K/IGF-1R signaling in human cancer cells. *International Journal of Biological Sciences*, *6*(6), 599–612.

Cheng, X., Yao, X., Xu, S., Pan, J., Yu, H., Bao, J., … Zhang, L. (2018). Punicalagin induces senescent growth arrest in human papillary thyroid carcinoma BCPAP cells via NF-κB signaling pathway. *Biomedicine & Pharmacotherapy*, *103*, 490–498. https://doi.org/10.1016/j.biopha.2018.04.074

Chua, K. F., Mostoslavsky, R., Lombard, D. B., Pang, W. W., Saito, S., Franco, S., … Alt, F. W. (2005). Mammalian SIRT1 limits replicative life span in response to chronic genotoxic stress. *Cell Metabolism*, *2*(1), 67–76. https://doi.org/10.1016/j.cmet.2005.06.007

Davenport, A. M., Huber, F. M., & Hoelz, A. (2014). Structural and functional analysis of human SIRT1. *Journal of Molecular Biology*, *426*(3), 526–541. https://doi.org/10.1016/j.jmb.2013.10.009

Dimri, G. P. (2005). What has senescence got to do with cancer? *Cancer Cell*, *7*, 505–512.

El Hasasna, H., Athamneh, K., Al Samri, H., Karuvantevida, N., Al Dhaheri, Y., Hisaindee, S., … Iratni, R. (2015). *Rhus coriaria* induces senescence and autophagic cell death in breast cancer cells through a mechanism involving p38 and ERK1/2 activation. *Scientific Reports*, *5*, 13013. https://doi.org/10.1038/srep13013

Eskelinen, E. L. (2006). Roles of LAMP-1 and LAMP-2 in lysosome biogenesis and autophagy. *Molecular Aspects of Medicine*, *27*(5-6), 495–502. https://doi.org/10.1016/j.mam.2006.08.005

Fang, Y., & Nicholl, M. B. (2011). Sirtuin 1 in malignant transformation: Friend or foe? *Cancer Letters*, *306*(1), 10–14. https://doi.org/10.1016/j.canlet.2011.02.019

Gewirtz, D. A. (2013). Autophagy and senescence in cancer therapy. *Journal of Cellular Physiology*, *229*(1), n/a–n/a. https://doi.org/10.1002/jcp.24420

Gewirtz, D. A., Holt, S. E., & Elmore, L. W. (2008). Accelerated senescence: An emerging role in tumor cell response to chemotherapy and radiation. *Biochemical Pharmacology*, *76*(8), 947–957. https://doi.org/10.1016/j.bcp.2008.06.024

Ghosh, D., Bhutia, S. K., Mallick, S. K., Banerjee, I., & Maiti, T. K. (2009). Stimulation of murine B and T lymphocytes by native and heat-denatured *Abrus agglutinin*. *Immunobiology*, *214*(3), 227–234. https://doi.org/10.1016/j.imbio.2008.08.002

Goehe, R. W., Di, X., Sharma, K., Bristol, M. L., Henderson, S. C., Valerie, K., … Gewirtz, D. A. (2012). The autophagy-senescence connection in chemotherapy: Must tumor cells (self) eat before they sleep? *Journal of Pharmacology and Experimental Therapeutics*, *343*(3), 763–778. https://doi.org/10.1124/jpet.112.197590

Hayflick, L. (1965). The limited in vitro lifetime of human diploid cell strains. *Experimental Cell Research*, *37*, 614–636.

Hegde, R., Maiti, T. K., & Podder, S. K. (1991). Purification and characterization of three toxins and two agglutinins from *Abrus precatorius* seed by using lactamyl-Sepharose affinity chromatography. *Analytical Biochemistry*, *194*(1), 101–109.

Huang, R., Xu, Y., Wan, W., Shou, X., Qian, J., You, Z., … Liu, W. (2015). Deacetylation of nuclear LC3 drives autophagy initiation under starvation. *Molecular Cell*, *57*(3), 456–466. https://doi.org/10.1016/j.molcel.2014.12.013

Huang, Y. H., Yang, P. M., Chuah, Q. Y., Lee, Y. J., Hsieh, Y. F., Peng, C. W., & Chiu, S. J. (2014). Autophagy promotes radiation-induced senescence but inhibits bystander effects in human breast cancer cells. *Autophagy*, *10*(7), 1212–1228. https://doi.org/10.4161/auto.28772

Jung, Y. R., Kim, E. J., Choi, H. J., Park, J. J., Kim, H. S., Lee, Y. J., … Lee, M. (2015). Aspirin targets SIRT1 and AMPK to induce senescence of colorectal carcinoma cells. *Molecular Pharmacology*, *88*(4), 708–719. https://doi.org/10.1124/mol.115.098616

Koga, T., Suico, M. A., Shimasaki, S., Watanabe, E., Kai, Y., Koyama, K., … Kai, H. (2015). Endoplasmic reticulum (ER) stress induces sirtuin 1 (SIRT1) expression via the PI3K-Akt-GSK3β signaling pathway and promotes hepatocellular injury. *Journal of Biological Chemistry*, *290*(290), 30366–30374.

Li, G., Rivas, P., Bedolla, R., Thapa, D., Reddick, R. L., Ghosh, R., & Kumar, A. P. (2013). Dietary resveratrol prevents development of high-grade prostatic intraepithelial neoplastic lesions: Involvement of SIRT1/S6K axis. *Cancer Prevention Research*, *6*(1), 27–39. https://doi.org/10.1158/1940-6207.capr-12-0349

Li, X., Wang, Y., Xiong, Y., Wu, J., Ding, H., Chen, X., … Zhang, H. (2016). Galangin Induces Autophagy via Deacetylation of LC3 by SIRT1 in HepG2 Cells. *Scientific Reports*, *6*, 30496. https://doi.org/10.1038/srep30496

Mukhopadhyay, S., Panda, P. K., Behera, B., Das, C. K., Hassan, M. K., Das, D. N., … Bhutia, S. K. (2014). In vitro and in vivo antitumor effects of Peanut agglutinin through induction of apoptotic and autophagic cell death. *Food and Chemical Toxicology*, *64*, 369–377. https://doi.org/10.1016/j.fct.2013.11.046

Mukhopadhyay, S., Panda, P. K., Das, D. N., Sinha, N., Behera, B., Maiti, T. K., & Bhutia, S. K. (2014). *Abrus* agglutinin suppresses human hepatocellular carcinoma in vitro and in vivo by inducing caspase-mediated cell death. *Acta Pharmacologica Sinica*, *35*(6), 814–824. https://doi.org/10.1038/aps.2014.15

Mukhopadhyay, S., Panda, P. K., Sinha, N., Das, D. N., & Bhutia, S. K. (2014). Autophagy and apoptosis: Where do they meet? *Apoptosis*, *19*(4), 555–566. https://doi.org/10.1007/s10495-014-0967-2

Mukhopadhyay, S., Schlaepfer, I. R., Bergman, B. C., Panda, P. K., Praharaj, P. P., Naik, P. P., … Bhutia, S. K. (2017). ATG14 facilitated lipophagy in cancer cells induce ER stress mediated mitoptosis through a ROS

dependent pathway. *Free Radical Biology and Medicine*, *104*, 199–213. https://doi.org/10.1016/j.freeradbiomed.2017.01.007

Naik, P. P., Das, D. N., Panda, P. K., Mukhopadhyay, S., Sinha, N., Praharaj, P. P., … Bhutia, S. K. (2016). Implications of cancer stem cells in developing therapeutic resistance in oral cancer. *Oral Oncology*, *62*, 122–135. https://doi.org/10.1016/j.oraloncology.2016.10.008

Ou, X., Lee, M. R., Huang, X., Messina-Graham, S., & Broxmeyer, H. E. (2014). SIRT1 positively regulates autophagy and mitochondria function in embryonic stem cells under oxidative stress. *Stem Cells*, *32*(5), 1183–1194. https://doi.org/10.1002/stem.1641

Panda, P. K., Behera, B., Meher, B. R., Das, D. N., Mukhopadhyay, S., Sinha, N., … Bhutia, S. K. (2017). Abrus agglutinin, a type II ribosome inactivating protein inhibits Akt/PH domain to induce endoplasmic reticulum stress mediated autophagy-dependent cell death. *Molecular Carcinogenesis*, *56*(2), 389–401. https://doi.org/10.1002/mc.22502

Panda, P. K., Mukhopadhyay, S., Das, D. N., Sinha, N., Naik, P. P., & Bhutia, S. K. (2015). Mechanism of autophagic regulation in carcinogenesis and cancer therapeutics. *Seminars in Cell & Developmental Biology*, *39*, 43–55. https://doi.org/10.1016/j.semcdb.2015.02.013

Panda, P. K., Naik, P. P., Meher, B. R., Das, D. N., Mukhopadhyay, S., Praharaj, P. P., … Bhutia, S. K. (2018). PUMA dependent mitophagy by Abrus agglutinin contributes to apoptosis through ceramide generation. *Biochimica et Biophysica Acta (BBA)—Molecular Cell Research*, *1865*(3), 480–495. https://doi.org/10.1016/j.bbamcr.2017.12.002

Panda, P. K., Naik, P. P., Praharaj, P. P., Meher, B. R., Gupta, P. K., Verma, R. S., … Bhutia, S. K. (2018). Abrusagglutinin stimulates BMP-2-dependent differentiation through autophagic degradation of β-catenin in colon cancer stem cells. *Molecular Carcinogenesis*, *57*(5), 664–677. https://doi.org/10.1002/mc.22791

Patel, K. R., Andreadi, C., Britton, R. G., Horner-Glister, E., Karmokar, A., Sale, S., … Brown, K. (2013). Sulfate metabolites provide an intracellular pool for resveratrol generation and induce autophagy with senescence. *Science Translational Medicine*, *5*(205), 205ra133. https://doi.org/10.1126/scitranslmed.3005870

Qi, M., Fan, S., Yao, G., Li, Z., Zhou, H., Tashiro, S., … Ikejima, T. (2013). Pseudolaric acid B-induced autophagy contributes to senescence via enhancement of ROS generation and mitochondrial dysfunction in murine fibrosarcoma L929 cells. *Journal of Pharmacological Sciences*, *121*(3), 200–211.

Riffelmacher, T., Clarke, A., Richter, F. C., Stranks, A., Pandey, S., Danielli, S., … Simon, A. K. (2017). Autophagy-dependent generation of free fatty acids is critical for normal neutrophil differentiation. *Immunity*, *47*(3), 466–480. https://doi.org/10.1016/j.immuni.2017.08.005

Schmitt, C. A., Fridman, J. S., Yang, M., Lee, S., Baranov, E., Hoffman, R. M., & Lowe, S. W. (2002). A senescence program controlled by p53 and p16INK4a contributes to the outcome of cancer therapy. *Cell*, *109*(3), 335–346.

Schönfeld, P., & Wojtczak, L. (2008). Fatty acids as modulators of the cellular production of reactive oxygen species. *Free Radical Biology and Medicine*, *45*(3), 231–241. https://doi.org/10.1016/j.freeradbiomed.2008.04.029

Settembre, C., & Ballabio, A. (2014). Lysosome: Regulator of lipid degradation pathways. *Trends in Cell Biology*, *24*(12), 743–750. https://doi.org/10.1016/j.tcb.2014.06.006

Shan, P., Fan, G., Sun, L., Liu, J., Wang, W., Hu, C., … Wang, C. (2017). SIRT1 functions as a negative regulator of eukaryotic poly(A)RNA transport. *Current Biology*, *27*(15), 2271–2284. https://doi.org/10.1016/j.cub.2017.06.040

Sinha, N., Panda, P. K., Naik, P. P., Das, D. N., Mukhopadhyay, S., Maiti, T. K., … Bhutia, S. K. (2017). Abrus agglutinin promotes irreparable DNA damage by triggering ROS generation followed by ATM-p73 mediated apoptosis in oral squamous cell carcinoma. *Molecular Carcinogenesis*, *56*(11), 2400–2413. https://doi.org/10.1002/mc.22679

Sinha, N., Panda, P. K., Naik, P. P., Maiti, T. K., & Bhutia, S. K. (2017). Abrus agglutinin targets cancer stem-like cells by eliminating self-renewal capacity accompanied with apoptosis in oral squamous cell carcinoma. *Tumour Biology*, *39*(5), 101042831770163. https://doi.org/10.1177/1010428317701634

Subburayan, K., Thayyullathil, F., Pallichankandy, S., Rahman, A., & Galadari, S. (2018). Par-4-dependent p53 up-regulation plays a critical role in thymoquinone-induced cellular senescence in human malignant glioma cells. *Cancer Letters*, *426*(80-97), 80–97. https://doi.org/10.1016/j.canlet.2018.04.009

Vargas, J., Feltes, B. C., Poloni Jde, F., Lenz, G., & Bonatto, D. (2012). Senescence; an endogenous anticancer mechanism. *Frontiers in Bioscience*, *17*, 2616–2643.

Xue, W., Zender, L., Miething, C., Dickins, R. A., Hernando, E., Krizhanovsky, V., … Lowe, S. W. (2007). Senescence and tumour clearance is triggered by p53 restoration in murine liver carcinomas. *Nature*, *445*(7128), 656–660. https://doi.org/10.1038/nature05529

Yang, Y. C., Chien, M. H., Liu, H. Y., Chang, Y. C., Chen, C. K., Lee, W. J., … Cheng, T. Y. (2018). Nuclear translocation of PKM2/AMPK complex sustains cancer stem cell populations under glucose restriction stress. *Cancer Letters*, *421*, 28–40. https://doi.org/10.1016/j.canlet.2018.01.075

Yao, Z. Q., Zhang, X., Zhen, Y., He, X. Y., Zhao, S., Li, X. F., … Duan, C. Z. (2018). A novel small-molecule activator of Sirtuin-1 induces autophagic cell death/mitophagy as a potential therapeutic strategy in glioblastoma. *Cell Death & Disease*, *9*(7), 767. https://doi.org/10.1038/s41419-018-0799-z

Young, A. R. J., Narita, M., Ferreira, M., Kirschner, K., Sadaie, M., Darot, J. F. J., … Narita, M. (2009). Autophagy mediates the mitotic senescence transition. *Genes & Development*, *23*(7), 798–803. https://doi.org/10.1101/gad.519709

Zhang, T., & Kraus, W. L. (2010). SIRT1-dependent regulation of chromatin and transcription: Linking NAD(+) metabolism and signaling to the control of cellular functions. *Biochimica et Biophysica Acta/General Subjects*, *1804*(8), 1666–1675. https://doi.org/10.1016/j.bbapap.2009.10.022

Zhang, Y., Dong, Y., Melkus, M. W., Yin, S., Tang, S. N., Jiang, P., & Jiang, C. (2018). Role of P53-senescence induction in suppression of LNCaP prostate cancer growth by cardiotonic compound bufalin. *Molecular Cancer Therapeutics*, *17*(11), 2341–2352. https://doi.org/10.1158/1535-7163.mct-17-1296

SUPPORTING INFORMATION

Additional supporting information may be found online in the Supporting Information section.

How to cite this article: Panda PK, Patra S, Naik PP, et al. Deacetylation of LAMP1 drives lipophagy-dependent generation of free fatty acids by *Abrus* agglutinin to promote senescence in prostate cancer. *J Cell Physiol*. 2019;1–16. https://doi.org/10.1002/jcp.29182